

An Efficient Metadynamics-Based Protocol to Model the Binding Affinity and the Transition State Ensemble of GPCR-Ligands

Noureldin Saleh,[‡] Passainte Ibrahim,[‡] Giorgio Saladino,[†] Francesco Luigi Gervasio^{†,§,} Timothy Clark^{‡,*}*

[‡] Computer-Chemie-Centrum and Interdisciplinary Center for Molecular Materials Friedrich-Alexander-Universität Erlangen-Nürnberg, Nögelsbachstraße 25, 91052 Erlangen, Germany.

[†] Department of Chemistry, University College London, London WC1H 0AJ, United Kingdom.

[§] Institute of Structural and Molecular Biology, University College London, London WC1E 6BT, United Kingdom.

E-mail: Tim.Clark@fau.de; f.l.gervasio@ucl.ac.uk

Abstract: A generally applicable metadynamics scheme for predicting the free-energy profile of ligand binding to G-protein coupled receptors (GPCRs) is described. A common and effective collective variable (CV) has been defined using the ideally placed and highly conserved Trp6.48 as a reference point for ligand-GPCR distance measurement and the common orientation of GPCRs in the cell membrane. Using this single CV together with well-tempered multiple-walker

metadynamics with a funnel-like boundary allows an efficient exploration of the entire ligand-binding path from the extracellular medium to the orthosteric binding site, including vestibule and intermediate sites. The protocol can be used with X-ray structures or high-quality homology models for the receptor and is universally applicable to agonists, antagonists, partial and reverse agonists. The root mean square error (RMSE) in predicted binding free energies for 12 diverse ligands in five receptors (a total of 23 data points) is surprisingly small (less than 1 kcal mol⁻¹). The RMSEs for simulations that use receptor X-ray structures and homology models are very similar.

Introduction

G-protein coupled receptors (GPCRs) represent the largest family of drug targets in drug discovery.¹ In the last decade, a number of GPCR crystal structures have been solved, greatly helping structure-based drug design (SBDD) for GPCRs, which was previously largely speculative or ligand-based.² Although it is now possible to use accurate explicit-solvent free-energy methods and enhanced-sampling (ES) atomistic simulations to predict the affinity and occasionally kinetics of ligand binding,^{3,4} the computational expense involved has hindered the use of such methods for routine SBDD in GPCRs. Docking, although sometimes successful in predicting protein-ligand complex geometries and despite its widespread use in drug design,⁵ suffers from simplified scoring functions⁶ and cannot model significant target conformational changes and accurate binding affinities and kinetics, which are important aspects for drug efficacy.⁷ Recent advances in hardware and force fields⁸ have made molecular-dynamics (MD) simulations an increasingly relevant tool for medicinal chemistry,^{8,9} although typical simulation times are not able to sample binding and unbinding events sufficiently.^{9,10} Enhanced sampling and free energy methods are intended to fill this gap. Free-energy perturbation¹¹ and

thermodynamic integration¹² have been successful in predicting relative, and sometimes even absolute, binding free energies but, due to their end-point approach, give no information about transition states and binding mechanisms. The metadynamics technique can be used to compute the binding free energy along physically meaningful pathways, predicting both the thermodynamics and kinetics of binding, and has established itself as the method of choice for free-energy prediction in complex molecular processes.^{3,13-24} However, metadynamics (and similar approaches) require the definition of one or more collective variables (CVs) that approximate the reaction coordinate, which must be chosen carefully.^{21,25,26} The time needed to converge a free energy profile increases significantly when poorly suited or too many CVs are selected. Using two or three CVs has so far proven to be an effective solution for studying protein-ligand interactions. Yet, even using metadynamics, several hundreds of nanoseconds, if not microseconds, of sampling are necessary to converge a free-energy profile fully.^{15-17,27} For GPCRs in particular, a recently published metadynamics protocol²⁸ requires 3-5 μ s average simulation time to converge one GPCR-ligand binding free-energy profile. What is more, when the ligand-binding mechanism requires complex target conformational changes, the use of multiple replica approaches (such as Parallel-Tempering Metadynamics or Hamiltonian-Replica Exchange Metadynamics) is necessary to converge the free energy landscape, making the calculation even more computationally expensive.²⁹⁻³¹ Thus, there is a clear need for computationally efficient metadynamics protocols for ligand binding to GPCRs. Ideally, such protocols should be accurate and inexpensive, so that turnaround times for binding free-energy profiles become suitable for routine SBDD-applications. To this end, optimal CVs that distinguish the bound, unbound and metastable states along the binding coordinate, while minimizing the exploration of unbound and weakly-bound states are very helpful.^{23,26,27,32}

Here, we report a simple, general and effective protocol that uses a smart and general CV together with recent advances in metadynamics to predict binding mechanisms and affinities accurately. We find these goals to be generally achievable in approximately 750 ns sampling time, which is now easily accessible on modern clusters and GPU machines.

A General and Effective Collective Variable

To define a general and effective CV, we selected a well-conserved extracellular residue, Trp6.48 and took the z -projection of its distance from the ligands (see Fig. 1). Trp6.48 is conserved in 90% of GPCRs and, unlike intracellular conserved residues in the NPxxY and DRY motifs, it is usually found lining the bottom of the binding pocket and its position does not vary much with the functional state of the GPCR. The highly conserved nature of the Trp6.48, previously believed to act as a rotameric switch,³³ allows the proposed CV to be used for different receptors and subtypes.¹⁸ This residue, is used to define a distance, as shown schematically in Figure 1. As the membrane is generally aligned to the xy -plane in MD simulations of GPCRs,³⁴ the projection on the z -axis of the distance between the relatively fixed C_α of Trp6.48 and the ammonium nitrogen of aminergic ligands (or an equivalent pharmacophore element), can be sufficient to describe the binding process (see Figure 1). Selecting a single, geometry-based CV that can be used with different ligands and different GPCRs is far from easy. The question of what is the minimum number of CVs needed to describe complex biological events, such as binding, is an open one. The intrinsic dimensionality of such events has been determined in a number of cases and the consensus is that for specific binding events a single effective CV can be devised. The problem is that in principle for each system and each ligand, a different CV might be needed. Increasing the number of reaction coordinates allows the exploration of binding events in different systems as it resolves

the problem of different states sharing the same reaction coordinate value and improves sampling of other slow degrees of freedom along the process investigated. However, increasing the dimensionality of the space to be explored through the addition of CVs comes at a large computational cost.

In the present case, we were able to define a simple and effective CV and have greatly reduced the number of states to be explored by implementing a funnel-shaped boundary. Extensive tests also showed that adding a second CV plays a negligible role in resolving overlapping states, since the ligands tend to be pre-oriented in the GPCR vestibule. The presence of the membrane, and the

alignment of the system, allow a bell-shaped funnel restraint to be applied to restrict the ligand to sampling relevant regions,¹⁷ instead of sampling the entirety of the bulk solvent. The funnel is applied as circular radii in the xy -plane centered on an axis in the z -direction over the relatively fixed C_α of Trp6.48 (see Figure 1). This approach is similar to “funnel metadynamics”,³² however, as in the case of the Path Collective Variables,²⁷ the boundary is defined in the target/membrane frame. Being rotationally invariant, it does not need any constraint on the rotation or translation of the system. We have found this simple setup to perform surprisingly well for all the GPCRs and ligands investigated in this work.

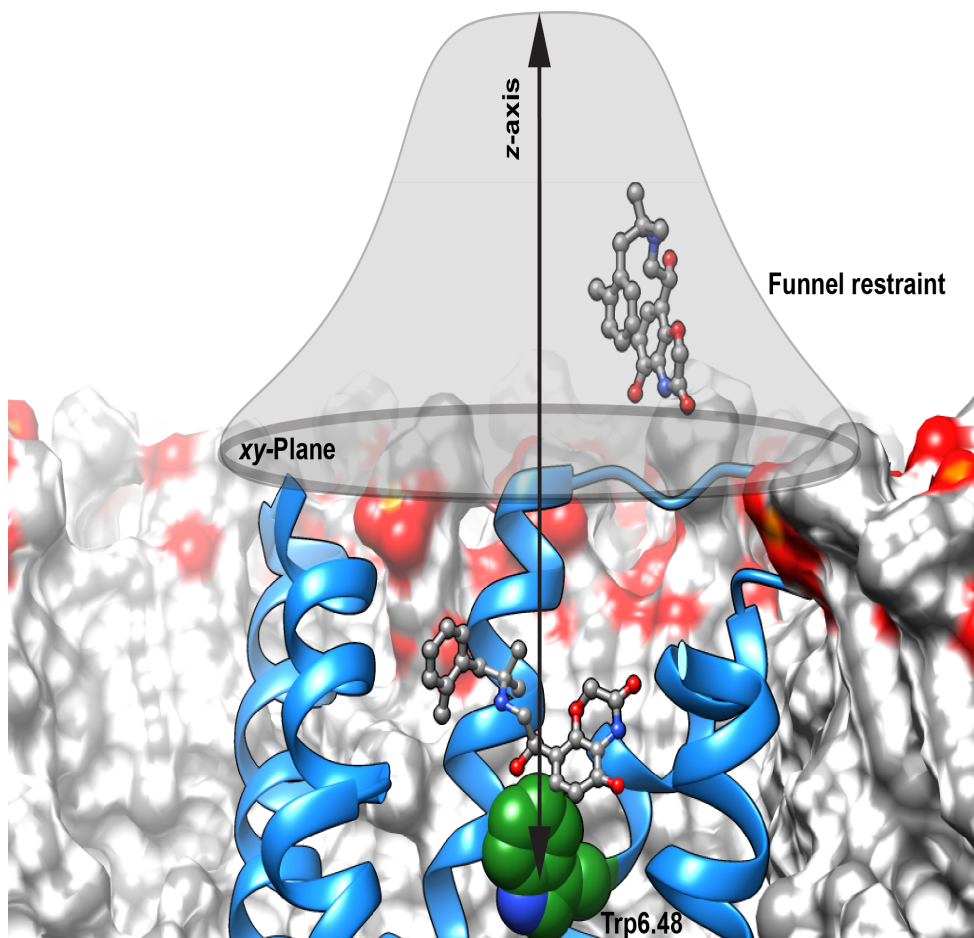


Figure 1. Scheme showing the definition of the CV and the of the funnel-shaped restraint with respect to the membrane and the GPCR (in blue) in the simulations. The membrane structure is used to define the *xy*-plane (gray circle), so that the *z*-component of the distance (black arrow) from the conserved Trp6.48 can be used effectively to describe the ligand binding. A bell-shaped funnel restraint, shown in translucent gray is used to speed up the convergence of the unbound-states exploration.

Recent simulations on a variety of GPCRs have shown that the extracellular vestibule of the receptor can pre-orient the ligand³⁴⁻³⁹ and thus provide a well-defined extracellular end-point for docking pathways, and thus simplifying the path-sampling task, often by a form of electrostatic focusing⁴⁰ but also by a simple mechanical effect in which part of the ligand is anchored,

decreasing the number of degrees of freedom to be sampled. This property of the extracellular region renders our simple CV quite effective; only a few pathways for GPCR-ligand binding are possible, the ligands find the right orientation during the sampling and binding sites along the path are identified and characterized reliably. As highly conserved residues lining the binding pocket might be identified in other membrane proteins, we believe that a similar simple approach might be used in other target families, beyond GPCRs.³²

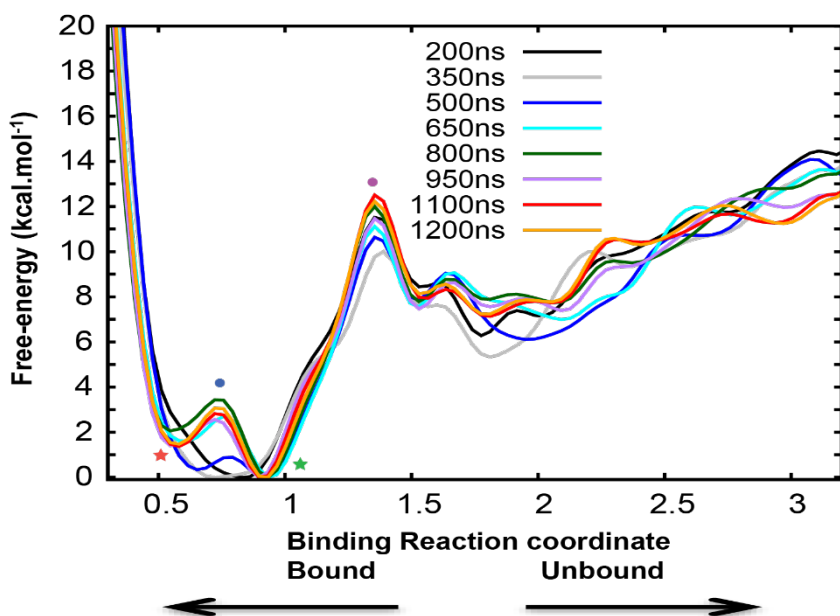


Figure 2. Binding free energy profiles of carvedilol reconstructed at increasing Metadynamics sampling times up to a maximum of 1250 ns (stars and circles in the top panel indicate the positions of minima and barriers monitored in the bottom panel). The change in the reconstructed free-energy profile is already $< 1 \text{ kcal mol}^{-1}$ after 500 ns. The free-energy differences between minima and between the minima and the barrier are fully converged after approximately 750 ns and 1 μs , respectively.

Additionally, to speed up the sampling, this approach can be easily combined with multiple-replica metadynamics approaches, such as parallel tempering²⁹ or the multiple-walker technique,³⁹ which uses several "walkers" to converge one free-energy profile. In our case, we found the trivially parallelizable (and asynchronous) multiple-walker approach more suitable as it is very flexible (the number of replicas can be dynamically changed to use the available resources) and ensures maximum computational efficiency even on non-homogenous clusters.

Computational Protocol

A preliminary metadynamics simulation is used to refine the poses and determine the one with the highest binding free energy, as described previously.⁴⁰ The ligand is first unbound using a faster protocol (see the Methods section for details). The position on the reaction coordinate at which the ligand is completely hydrated and unbound is determined and representative structures are extracted from the simulation for each 2Å window along the reaction coordinate from the docked pose to the unbound state. A multiple-walker funnel-metadynamics simulation with an appropriate bias factor of 20, Gaussian hills of 0.48 kcal mol⁻¹ and hill-width of 1 Å, is then started using the geometries extracted from the preliminary metadynamics run. A full free-energy profile is usually converged in 0.5 to 1 μs of collective simulation time, depending on the number of replicas, approximately 30-50 ns per replica (see Figures 2 and S3). The slow filling of the energy basins together with the funnel-shaped boundary and self-healing nature of the free-energy landscapes reconstructed by metadynamics¹⁹ helps explore the relevant poses along the (un)binding coordinate. This was also demonstrated by the ability of the metadynamics scheme to predict the crystallographic binding modes of BI-167107 and alprenolol in inactive ADRB2 starting with both ligands in the extracellular solvent phase (see Supplementary Movies M1 and M2).

Figure 2 shows the overall change in the free-energy profiles as a function of increasing sampling time for carvedilol. The first three curves (250, 350 and 500 ns) deviate significantly from one another and from the later curves. From 500 ns of sampling onwards the reconstructed profiles start to converge, attaining constant ΔG for the minima after 750 ns and 1 μ s for the barriers. The convergence behavior of the other systems is similar, as can be seen from Fig. S3. This convergence is due to multiple re-crossing events (Fig. S4) and the enhancement of sampling by multiple walkers (Fig. S5).

Results

We have tested the above protocol on a set of 23 GPCR-ligand pairs consisting of five receptors in three different conformational states (G-protein stabilized, nanobody stabilized and binary complex) and 12 ligands that bind to three different sites (orthosteric, intermediate and vestibule, i.e. allosteric).¹⁸ The results are summarized in Table 1 and Figure 3 (full profiles are shown in supplementary Figure S2). Among all ligands, 10 act on the respective receptors as agonist, 11 as antagonist and 2 as partial agonist. The initial receptor geometries were taken from X-ray geometries for the β 2-adrenergic receptor (ADRB2),⁴¹⁻⁴⁴ muscarinic M2 receptor (M2R)^{36,45} and μ -opioid receptor (μ OR)^{46,47} and are based on homology models¹⁸ for the vasopressin receptors $V_{1a}R$ and V_2R . The ADRB2, M2R and μ OR receptors were added to our existing data for the vasopressin receptor, as they were the only receptors crystallized in both the active and inactive states, and for which agonist-affinities to both the active (G-protein stabilized and nanobody stabilized) and inactive states were available when the study was conceived. Additionally, ligands with a broad range of intrinsic activity have been co-crystallized with ADRB2 and affinities determined in different functional states of the receptor.⁴¹⁻⁴⁴

Figure 2 shows a representative reconstructed binding free-energy profile. The profile is for carvedilol, which is considered a partial agonist on the arrestin pathway and inverse agonist on the G-protein pathway. We have previously shown in reference 18 that ligands with partial agonistic efficacy can occupy minima energetically close to the global minimum. The results in the table include the global minimum for the most stable binding state determined from the free-energy profiles shown in Supplementary Figure S2.

Table 1. List of the complexes used for the metadynamics simulations and their experimental and calculated binding free energies (in kcal mol⁻¹). Experimental free energies are obtained from the relation $\Delta G = -RT \ln(K_i)$ at $T=298$ K and the computed ones as described in the Methods section. All values are corrected for standard volume and funnel potential used as described in reference 27. The receptors whose structures were based on homology models are indicated by asterisks.

Ligand	Receptor	Effect	System	Binding site	K _i (nM)	$\Delta G_{\text{exp.}}$	$\Delta G_{\text{calc.}}$
Conivaptan	V1aR*	Antagonist	Binary	Intermediate	0.43 ⁴⁹	-13.0	-11.5±0.9
Lixivaptan	V1aR*	Antagonist	Binary	Intermediate	44 ⁵⁰	-10.1	-9.5±1.7
MCF18	V1aR*	Partial agonist	Binary	<u>Intermediate/</u> orthosteric	106 ⁵¹	-9.6	-9.1±1.2
Conivaptan	V2R*	Antagonist	Binary	Vestibule	0.36 ⁴⁹	-12.9	-11.4±0.5
Lixivaptan	V2R*	Antagonist	Binary	Vestibule	2.3 ⁵⁰	-11.9	-10.7±0.2
Satavaptan	V2R*	Antagonist	Binary	Vestibule	0.54 ⁵²	-12.7	-11.0±0.7
MCF18	V2R*	Partial agonist	Binary	<u>Vestibule/</u> orthosteric	20 ⁵¹	-10.5	-10.0±2.3
Satavaptan	V1aR*	Antagonist	Binary	Orthosteric	460 ⁵²	-8.7	-9.1±1.1
Iperoxo	M2R	Agonist	Ternary-G _i	Orthosteric	0.01 ³⁶	-15.1	-15.7±0.8
Iperoxo	M2R	Agonist	Ternary-	Orthosteric	0.1 ³⁶	-13.7	-13.4±0.8

			nanobody				
Iperoxo	M2R	Agonist	Binary	Orthosteric	10^{36}	-11.0	-11.5±0.7
BU72	μOR	Agonist	Ternary-G _i	Orthosteric	0.021 ⁴⁷	-14.8	-14.6±0.6
BU72	μOR	Agonist	Ternary-nanobody	Orthosteric	0.016 ⁴⁷	-15.1	-15.5±0.9
BU72	μOR	Agonist	Binary	Orthosteric	0.47 ⁴⁷	-12.8	-13.7±1.1
ICI-188551	ADRB2	Antagonist	Binary	Orthosteric	1 ⁵³	-12.8	-13.5±0.2
Alprenolol	ADRB2	Antagonist	Binary	Orthosteric	1.2 ⁵³	-12.7	-14.1±0.3
Carvedilol	ADRB2	Antagonist	Binary	Orthosteric	1.1 ⁵⁴	-12.7	-13.9±0.8
Isoprenaline	ADRB2	Agonist	Binary	Orthosteric	107 ⁴³	-9.9	-11.1±0.4
BI-167107	ADRB2	Agonist	Binary	Orthosteric	0.084 ⁴³	-14.3	-14.9±0.6
Adrenaline	ADRB2	Agonist	Binary	Orthosteric	124 ⁵⁵	-9.8	-11.4±0.1
Isoprenaline	ADRB2	Agonist	Ternary-G _s	Orthosteric	1.07 ⁴³	-12.7	-13.3±0.8
Adrenaline	ADRB2	Agonist	Ternary-G _s	Orthosteric	0.246 ⁵⁵	-13.6	-15.1±0.3
ICI-188551	ADRB2	Antagonist	Ternary-G _s	Orthosteric	10 ⁵³	-11.3	-12±1.3

Table 2. Error metrics for the comparison between experimental and calculated binding free energies (kcal mol⁻¹) shown in Table 1 and Figure 2. “Homology” and “X-ray” define the source of the initial structure for the receptor.

	All	Homology	X-ray
Mean signed error, MUE	0.2	-0.8	0.8
Mean unsigned error, MUE	0.9	1.0	0.8
Root mean square error, RMSE	1.0	1.1	1.0
Most positive error	1.7	0.4	1.7
Most negative error	-1.7	-1.7	-0.3

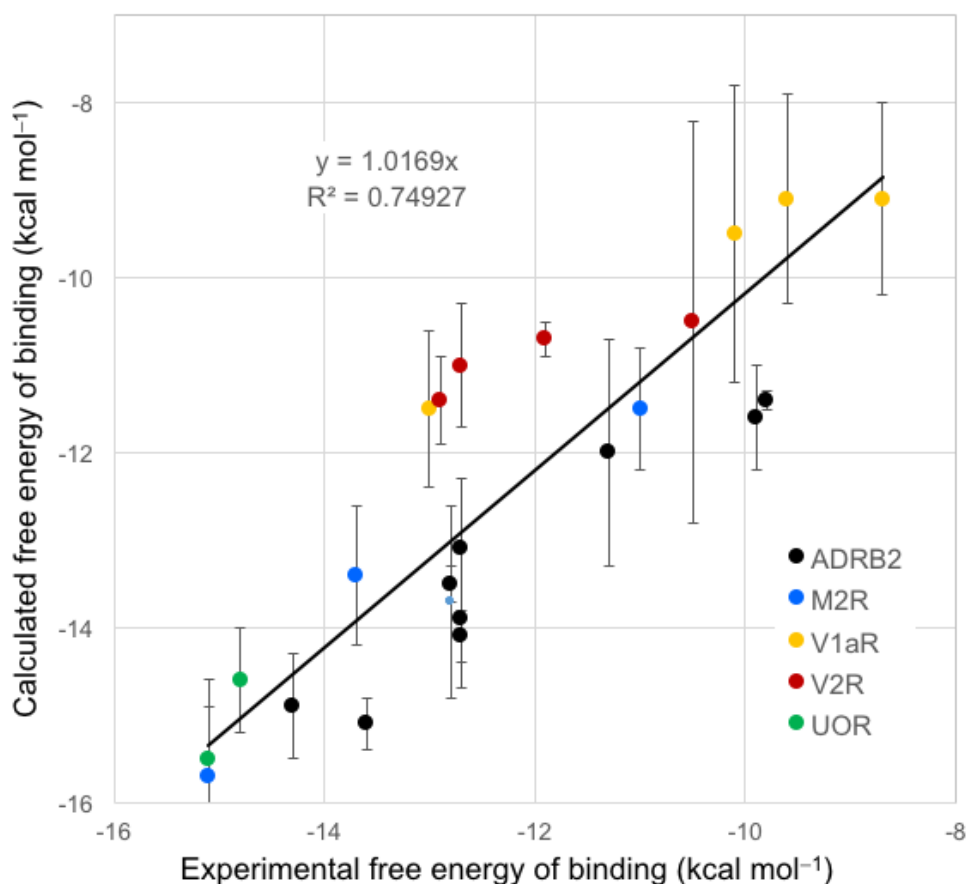


Figure 3. Correlation between the experimental and calculated binding free energies for the data shown in Table 1.

The calculated binding free energies show good agreement with experiment with a maximum absolute error of 2 kcal mol⁻¹ and an overall root mean square error (RMSE) of less than 1 kcal mol⁻¹. The regression between the experimental and calculated binding free energies (without a constant term) exhibits a coefficient of determination (R^2) of 0.749 for the entire dataset with a slope of 1.02, reassuringly close to unity. The statistics of the fit between experiment and simulations is shown in Table 2 for the entire dataset, and for the data points based on X-ray

structures and homology models of the receptors separately. The errors for simulations using X-ray receptor structures are very similar to those calculated using homology models (RMSE 1.0 vs. 1.1 kcal mol⁻¹). We thus conclude that the metadynamics protocol described here is able to reproduce the binding thermodynamics of GPCR-ligands accurately, irrespective of whether the receptor structure is based on X-ray crystallography or a well-equilibrated homology model (based on a highly homologous template, in this case 31% sequence similarity). Quite remarkably, this conclusion applies to all types of ligand (agonist, antagonist, inverse agonist) and multiple binding sites. While other enhanced sampling methods, as Gaussian-accelerated MD, which allows the simultaneous biasing of a large number of CVs, have been successful in simulating spontaneous binding of ligands to GPCRs,⁵⁶ they are generally less efficient in sampling the full dissociation of strongly bound ligands.

Conclusions

We have described a robust metadynamics protocol that performs well in reproducing the free energies of binding of a variety of ligands with different effects on five different GPCRs. The metadynamics protocol performs similarly for agonists (11 data points), antagonists (10) and partial agonists (2), even though antagonists bind to two alternative sites and the partial agonists bind in equilibrium between the orthosteric and one other site. Three different types of binding site are considered for the five receptors. The data shown in Tables 1 and 2 and Figure 3 provide convincing evidence that the protocol described can predict free energies of binding for all types of GPCR ligand with an accuracy of approximately ± 1 kcal mol⁻¹, regardless of whether an X-ray structure or a homology model is used as the original structure source for the receptor and provided that this model has been equilibrated by μ s-scale MD simulations.

Materials and Methods:

General set up of MD simulations

Topologies for the receptors were generated using the AMBER99SB-ILDN force field⁵⁷ and inserted into a pre-equilibrated dioleoylphosphatidylcholine (DOPC) bilayer⁵⁸ according to the orientation in the OPM database⁵⁹ using the GROMACS tool `g_membed`.⁶⁰ Ligands were parameterized using the generalized AMBER force field (GAFF)^{61,62} together with AM1-BCC partial charges.⁶² The appropriate number of sodium and chloride ions was added to the systems to simulate a physiological salt concentration of 100mM. Particle-mesh Ewald (PME)⁶³ was used to treat electrostatic interactions, using a cut-off distance of 10 Å. The resulting system was geometry-optimized and then equilibrated for 10 ns followed by a production run. All simulations used the SPC/E water model.⁶⁴ All simulations were performed using GROMACS⁶⁵ with the PLUMED plug-in⁶⁶ for the metadynamics simulations. The simulations of the ternary complexes used a box size of 95×95×160 Å with 37,000 water molecules, and 239 DOPC molecules, whereas the binary systems comprised a box of 95×95×115 Å with 21,000 water molecules and 239 DOPC molecules.

β₂-adrenergic receptor (ADRB2)

The inactive β₂ receptor was modeled based on the high-resolution crystal structure (PDB access code 2RH1⁴¹). The model was then equilibrated for 10 ns at constant pressure (NPT) and simulated for 500 ns of production MD simulation. A ternary complex model for ADRB2 with the BI-167107 agonist and the G_{αs} subunit of the G-protein after 500ns MD simulation,⁶⁷ based on the ternary complex structure of ADRB2 (PDB access code 3SN6⁴³) was used.⁶⁷ The active-

state structure of the ADRB2-adrenaline complex stabilized by a nanobody,⁵⁵ was aligned to our first ternary model and the adrenaline coordinates were transferred to obtain an adrenaline pose consistent with the ternary complex. The adrenaline-ADRB2-G_{αs} ternary complex was equilibrated and simulated for one μs. The stabilizing NB6B9 nanobody was transferred from the adrenaline-stabilized active-state ADRB2 to our ADRB2 structure and the G_{αs} was deleted. The model was then equilibrated for 500 ns MD simulation.

The crystal structures of ADRB2 bound to the inverse agonist ICI 118,551 (PDB access code 3NY8⁴²), ADRB2 bound to the antagonist alprenolol (PDB access code 3NYA⁴²), ADRB1 bound to the agonist isoprenaline (PDB access code 2Y03⁶⁸) and ADRB1 bound to the biased agonist carvedilol (PDB access code 4AMJ⁶⁹), were aligned to the inactive, binary and active, ternary-G_{αs} models of ADRB2 after 500ns MD equilibration based on the C_α atoms of the residues within 5 Å of the binding pocket of each ligand. The ligand coordinates were transferred to the inactive models, which were then equilibrated for 500 ns of MD simulation.

M₂ Muscarinic acetylcholine receptor

A ternary iperoxo-M₂R-nanobody9-8 (Nb9-8) complex model was based on the crystal structure of active-state M₂R (PDB access code 4MQS³⁶). A model for the G_{αi}-protein was constructed, using a previously published model for nucleotide-free G_i in complex with the D₂ dopaminergic receptor.⁶⁷ The D₂-G_{αi} ternary complex was aligned to the ADRB2-G_{αs} complex and the M₂-iperoxo complex, followed by substituting the Nb9-8 with the G_{αi}. The final models were then aligned in the membrane according to the orientation in the OPM database.⁵⁹ All the models were then equilibrated and simulated for one μs.

μ-opioid receptor

A ternary BU72-μOR-nanobody39 (Nb39) complex model was based on the crystal structure of active-state μOR (PDB access code 5C1M⁴⁷). A model for the G_{αi}-protein was constructed, using a previously published model for active-state G_i in complex with the D₂ dopaminergic receptor.⁶⁷ The D₂-G_{αi} ternary complex was aligned to the ADRB2-G_{αs} complex and the BU72-μOR complex, followed by substituting the Nb9-8 with the G_{αi}.

The two crystal structures (PDB access codes 4DKL⁴⁶ and 5C1M⁴⁷), are complementary with respect to missing substructures. The missing N-terminal and ICL3 substructures in the inactive model and the missing helix 8 of the active model were modeled using the resolved structure in the other partner. The final models were then aligned in the membrane according to the orientation in the OPM database.⁵⁹ All the models were then equilibrated and simulated for one μs.

Vasopressin V₂ receptor

Details of the homology modeling, simulations and methods are given in reference 18. The homology model was based on the NTS₁ structure (PDB accession code: 4GRV,⁷¹ sequence similarity 31%), built using the Modeller software and ranked based on their DOPE score.^{72,73} Its quality was found to be good by two different tools (Verify3D and Eval23D).^{74,75}

Metadynamics simulations of ligand binding to *μ-opioid*, muscarinic M₂ and β₂ adrenergic receptors.

Metadynamics simulations were performed in order to obtain estimates of the binding free-energy profiles. We used a combination of the well-tempered metadynamics (WT)^{21,70} and funnel-shaped walls in the spirit of Path collective Variables (PCV) and funnel metadynamics

(FM).³² A metadynamics history-dependent bias was applied along the component of the z -distance between the relatively fixed C_α of Trp6.48 deep in the binding region and the center ammonium nitrogen of the ligands. This distance was used as the single collective variable. The funnel restraint was then applied to the relative position on the xy -plane (restrained to 8 Å radius when fully unbound and allowing 13 Å radius if around the vestibule or deeper) to ensure better sampling for the relevant region of the free energy, as the ligand can otherwise move extensively in the extracellular solvent without affecting the free energy. Gaussian hills with initial height of 0.48 kcal mol⁻¹ applied every 1 ps were used. The hill width was chosen to be 1 Å. The Gaussian functions were rescaled in the WT scheme using a bias factor of 20. Initial metadynamics simulations were performed with the same parameters, except for a higher bias factor of 30. Representative structures were extracted from the simulation for each 2 Å window, and used as starting coordinates for the multiple walker technique.³⁹ This ensured faster convergence of the free-energy surface and enhanced the parallelization. The free energies were calculated using the `sum_hills` function of the PLUMED plug-in⁶⁶ and corrected for the loss of translational and rotational freedom of the unbound ligand due to the funnel-like boundaries according to the following equations:

$$\Delta G_{\text{binding}} = \Delta G_{\text{meta}} + \text{Funnel/standard Volume Correction}$$

$$\Delta G_{\text{meta}} = K_B T \log \left(\frac{\int_{\text{Bound}} ds \exp\left(\frac{-F(s)}{K_B T}\right)}{\int_{\text{Unbound}} ds \exp\left(\frac{-F(s)}{K_B T}\right)} \right)$$

, where the bound states were defined by the position of the global minimum and the unbound states by values of the distance CV greater than 28 Å. An upper-limit for the CV was set at 35 Å, based on the box size and available solvent phase and to avoid interactions with the intracellular

side of the receptor. The correction for the standard volume and funnel restraint was computed as described in references 76 and 77 according to the formula:

$$\text{Funnel/standard Volume Correction} = -RT \ln \left(\frac{\xi_{\text{bulk}}^{\text{meta}} V_{\text{bulk}}^{\text{meta}} V_{\text{box}}}{8\pi V_{\text{bulk}} V_0} \right)$$

ξ_{bulk} is the fraction of the total possible orientations explored by the ligand in the unbound state. V_0 is the standard volume accessible to a ligand at 1 mol L⁻¹ concentration, and V_{bulk} is the bulk volume (i.e., $V_{\text{box}} - V_{\text{protein+membrane}}$). The correction was found to range from ~ 0.4 to ~0.6 kcal mol⁻¹ for the binary and ternary systems.

Error estimation

Error estimates were calculated using a script implementing a variant of Ref. 48 reweight algorithm (available here <https://www.ucl.ac.uk/chemistry/research/research-groups/group-folder/protein-dynamics-francesco-gervasio/software>). The script uses the time dependent 1) free-energy profiles calculated every 50 ns after the initial exploration phase and 2) the time-independent free-energy profile obtained from the reweighting procedure. The error estimate is then determined as the average difference of the two.

The sampling/convergence errors for the calculated values were also estimated in the classical manner by comparing the free-energy differences obtained after different sampling times. The two estimates are in good agreement.

Supporting Information

The Supporting Information is available free of charge on the ACS Publications website.

Supplementary figures referred to in the main text.

Acknowledgements

This work was supported by the *Deutsche Forschungsgemeinschaft* as part of *GRK1910* “Medicinal Chemistry of Selective GPCR Ligands” and by a generous grant of computer time on SuperMUC at the *Leibniz Rechenzentrum*, Munich (projects pr94to and pr74su). GS and FLG acknowledge EPSRC [grant no EP/M013898/1] for financial support.

References

1. Hopkins, A. L.; Groom, C. R., The Druggable Genome. *Nature Rev. Drug Disc.* **2002**, *1*, 727-730.
2. Bertheleme, N.; Chae, P. S.; Singh, S.; Mossakowska, D.; Hann, M. M.; Smith, K. J.; Hubbard, J. A.; Dowell, S. J.; Byrne, B., Unlocking the Secrets of the Gatekeeper: Methods for Stabilizing and Crystallizing GPCRs. *Biochim. Biophys. Acta* **2013**, *1828*, 2583-2591.
3. Juraszek, J.; Saladino, G.; van Erp, T. S.; Gervasio, F. L., Efficient Numerical Reconstruction of Protein Folding Kinetics with Partial Path Sampling and Pathlike Variables. *Phys. Rev. Lett.* **2013**, *110*, 108106.
4. Tiwary, P.; Limongelli, V.; Salvalaglio, M.; Parrinello, M., Kinetics of Protein-Ligand Unbinding: Predicting Pathways, Rates, and Rate-Limiting Steps. *Proc. Nat. Acad. Sci. USA* **2015**, *112*, E386-391.
5. Neves, M. A.; Totrov, M.; Abagyan, R., Docking and Scoring with ICM: The Benchmarking Results and Strategies for Improvement. *J. Comp.-Aid Mol. Des.* **2012**, *26*, 675-686.
6. Warren, G. L.; Andrews, C. W.; Capelli, A. M.; Clarke, B.; LaLonde, J.; Lambert, M. H.; Lindvall, M.; Nevins, N.; Semus, S. F.; Senger, S.; Tedesco, G.; Wall, I. D.; Woolven, J. M.; Peishoff, C. E.; Head, M. S., A Critical Assessment of Docking Programs and Scoring Functions. *J. Med. Chem.* **2006**, *49*, 5912-5931.
7. Pan, A. C.; Borhani, D. W.; Dror, R. O.; Shaw, D. E., Molecular Determinants of Drug-Receptor Binding Kinetics. *Drug Disc. Today* **2013**, *18*, 667-673.
8. Dror, R. O.; Dirks, R. M.; Grossman, J. P.; Xu, H.; Shaw, D. E., Biomolecular Simulation: A Computational Microscope for Molecular Biology. *Ann. Rev. Biophys.* **2012**, *41*, 429-452.
9. Hansson, T.; Oostenbrink, C.; van Gunsteren, W., Molecular Dynamics Simulations. *Curr. Opin. Struct. Biol.* **2002**, *12*, 190-196.
10. Zuckerman, D. M., Equilibrium Sampling in Biomolecular Simulations. *Ann. Rev. Biophys.* **2011**, *40*, 41-62.
11. Zwanzig, R. W., High-Temperature Equation of State by a Perturbation Method. I. Nonpolar Gases. *J. Chem. Phys.* **1954**, *22*, 1420.

12. Pearlman, D. A.; Charifson, P. S., Are Free Energy Calculations Useful in Practice? A Comparison with Rapid Scoring Functions for the p38 MAP Kinase Protein System. *J. Med. Chem.* **2001**, *44*, 3417-3423.
13. Morando, M. A.; Saladino, G.; D'Amelio, N.; Pucheta-Martinez, E.; Lovera, S.; Lelli, M.; Lopez-Mendez, B.; Marenchino, M.; Campos-Olivas, R.; Gervasio, F. L., Conformational Selection and Induced Fit Mechanisms in the Binding of an Anticancer Drug to the c-Src Kinase. *Sci. Rep.* **2016**, *6*, 24439.
14. Pucheta-Martinez, E.; Saladino, G.; Morando, M. A.; Martinez-Torrecedrada, J.; Lelli, M.; Sutto, L.; D'Amelio, N.; Gervasio, F. L., An Allosteric Cross-Talk Between the Activation Loop and the ATP Binding Site Regulates the Activation of Src Kinase. *Sci. Rep.* **2016**, *6*, 24235.
15. Limongelli, V.; Bonomi, M.; Marinelli, L.; Gervasio, F. L.; Cavalli, A.; Novellino, E.; Parrinello, M., Molecular basis of cyclooxygenase enzymes (COXs) selective inhibition. *Proc. Nat. Acad. Sci. USA* **2010**, *107*, 5411-5416.
16. Grazioso, G.; Limongelli, V.; Branduardi, D.; Novellino, E.; De Micheli, C.; Cavalli, A.; Parrinello, M., Investigating the Mechanism of Substrate Uptake and Release in the Glutamate Transporter Homologue Glt(Ph) through Metadynamics Simulations. *J. Am. Chem. Soc.* **2012**, *134*, 453-463.
17. Troussicot, L.; Guilliere, F.; Limongelli, V.; Walker, O.; Lancelin, J. M., Funnel-Metadynamics and Solution NMR to Estimate Protein-Ligand Affinities. *J. Am. Chem. Soc.* **2015**, *137*, 1273-1281.
18. Saleh, N.; Saladino, G.; Gervasio, F. L.; Haensele, E.; Banting, L.; Whitley, D. C.; Sopkova-de Oliveira Santos, J.; Bureau, R.; Clark, T., A Three-Site Mechanism for Agonist/Antagonist Selective Binding to Vasopressin Receptors. *Angew. Chem. Int. Ed.* **2016**, *55*, 8008-8012.
19. Sutto, L.; Gervasio, F. L., Effects of oncogenic mutations on the conformational free-energy landscape of EGFR kinase. *Proc. Nat. Acad. Sci. USA* **2013**, *110*, 10616-10621.
20. Tiwary, P.; Parrinello, M., From Metadynamics to Dynamics. *Phys. Rev. Lett.* **2013**, *111*, 230602.
21. Laio, A.; Parrinello, M., Escaping Free-Energy Minima. *Proc. Nat. Acad. Sci. USA* **2002**, *99*, 12562-12566.
22. Laio, A.; Gervasio, F. L., Metadynamics: A Method to Simulate Rare Events and Reconstruct the Free Energy in Biophysics, Chemistry and Material Science. *Rep. Prog. Phys.* **2008**, 122601.
23. Masetti, M.; Cavalli, A.; Recanatini, M.; Gervasio, F. L., Exploring Complex Protein-Ligand Recognition Mechanisms with Coarse Metadynamics. *J. Phys. Chem. B* **2009**, *113*, 4807-4816.
24. Cavalli, A.; Spitaleri, A.; Saladino, G.; Gervasio, F. L., Investigating Drug-Target Association and Dissociation Mechanisms Using Metadynamics-Based Algorithms. *Acc. Chem. Res.* **2015**, *48*, 277-285.

25. Barducci, A.; Bonomi, M.; Parrinello, M., Metadynamics. *Wires Comput Mol Sci* **2011**, *1*, 826-843.
26. Branduardi, D.; Gervasio, F. L.; Parrinello, M., From A to B in Free Energy Space. *J. Chem. Phys.* **2007**, *126*, 054103.
27. Saladino, G.; Gauthier, L.; Bianciotto, M.; Gervasio, F. L., Assessing the Performance of Metadynamics and Path Variables in Predicting the Binding Free Energies of p38 Inhibitors. *J Chem. Theory Comput.* **2012**, *8*, 1165-1170.
28. Schneider, S.; Provasi, D.; Filizola, M., The Dynamic Process of Drug-GPCR Binding at Either Orthosteric or Allosteric Sites Evaluated by Metadynamics. *Meth. Mol. Biol.* **2015**, 1335, 277-294.
29. Bussi, G.; Gervasio, F. L.; Laio, A.; Parrinello, M., Free-Energy Landscape for β -Hairpin Folding from Combined Parallel Tempering and Metadynamics. *J. Am. Chem. Soc.* **2006**, *128*, 13435-13441.
30. Lovera, S.; Morando, M.; Pucheta-Martinez, E.; Martinez-Torrecuadrada, J. L.; Saladino, G.; Gervasio, F. L., Towards a Molecular Understanding of the Link between Imatinib Resistance and Kinase Conformational Dynamics. *PLoS Comput. Biol.* **2015**, *11*, e1004578.
31. Bonomi, M.; Gervasio, F. L.; Tiana, G.; Provasi, D.; Broglia, R. A.; Parrinello, M. Insight into the Folding Inhibition of the HIV-1 Protease by a Small Peptide. *Biophys. J.* **2007**, *93*, 2813-2821
32. Limongelli, V.; Bonomi, M.; Parrinello, M., Funnel metadynamics as accurate binding free-energy method. *Proc. Nat. Acad. Sci. USA* **2013**, *110*, 6358-6363.
33. Mirzadegan, T.; Benko, G.; Filipek, S.; Palczewski, K., Sequence Analyses of G-Protein-Coupled Receptors: Similarities to Rhodopsin. *Biochem.* **2003**, *42*, 2759-2767.
34. Dror, R. O.; Pan, A. C.; Arlow, D. H.; Borhani, D. W.; Maragakis, P.; Shan, Y.; Xu, H.; Shaw, D. E., Pathway and Mechanism of Drug Binding to G-Protein-Coupled Receptors. *Proc. Nat. Acad. Sci. USA* **2011**, *108*, 13118-13123.
35. Dror, R. O.; Green, H. F.; Valant, C.; Borhani, D. W.; Valcourt, J. R.; Pan, A. C.; Arlow, D. H.; Canals, M.; Lane, J. R.; Rahmani, R.; Baell, J. B.; Sexton, P. M.; Christopoulos, A.; Shaw, D. E., Structural Basis for Modulation of a G-Protein-Coupled Receptor by Allosteric Drugs. *Nature* **2013**, *503*, 295-299.
36. Kruse, A. C.; Ring, A. M.; Manglik, A.; Hu, J.; Hu, K.; Eitel, K.; Hubner, H.; Pardon, E.; Valant, C.; Sexton, P. M.; Christopoulos, A.; Felder, C. C.; Gmeiner, P.; Steyaert, J.; Weis, W. I.; Garcia, K. C.; Wess, J.; Kobilka, B. K., Activation and Allosteric Modulation of a Muscarinic Acetylcholine Receptor. *Nature* **2013**, *504*, 101-106.
37. Kappel, K.; Miao, Y.; McCammon, J. A., Accelerated Molecular Dynamics Simulations of Ligand Binding to a Muscarinic G-Protein-Coupled Receptor. *Quart. Rev. Biophys.* **2015**, *48*, 479-487.
38. Miao, Y.; McCammon, J. A., Graded Activation and Free Energy Landscapes of a Muscarinic G-Protein-Coupled Receptor. *Proc. Nat. Acad. Sci. USA* **2016**, *113*, 12162-12167.

39. Raiteri, P.; Laio, A.; Gervasio, F. L.; Micheletti, C.; Parrinello, M., Efficient Reconstruction of Complex Free Energy Landscapes by Multiple Walkers Metadynamics. *J.Phys. Chem. B* **2006**, *110*, 3533-3539.
40. Milanos, L.; Saleh, N.; Kling, R. C.; Kaindl, J.; Tschammer, N.; Clark, T., Identification of Two Distinct Sites for Antagonist and Biased Agonist Binding to the Human Chemokine Receptor CXCR3. *Angew. Chem. Int. Ed.* **2016**, *55*, 15277-15281.
41. Cherezov, V.; Rosenbaum, D. M.; Hanson, M. A.; Rasmussen, S. G.; Thian, F. S.; Kobilka, T. S.; Choi, H. J.; Kuhn, P.; Weis, W. I.; Kobilka, B. K.; Stevens, R. C., High-Resolution Crystal Structure of an Engineered Human β 2-Adrenergic G Protein-Coupled Receptor. *Science* **2007**, *318*, 1258-1265.
42. Wacker, D.; Fenalti, G.; Brown, M. A.; Katritch, V.; Abagyan, R.; Cherezov, V.; Stevens, R. C., Conserved Binding Mode of Human β 2 Adrenergic Receptor Inverse Agonists and Antagonists Revealed by X-Ray Crystallography. *J. Am. Chem. Soc.* **2010**, *132*, 11443-11445.
43. Rasmussen, S. G.; DeVree, B. T.; Zou, Y.; Kruse, A. C.; Chung, K. Y.; Kobilka, T. S.; Thian, F. S.; Chae, P. S.; Pardon, E.; Calinski, D.; Mathiesen, J. M.; Shah, S. T.; Lyons, J. A.; Caffrey, M.; Gellman, S. H.; Steyaert, J.; Skiniotis, G.; Weis, W. I.; Sunahara, R. K.; Kobilka, B. K., Crystal Structure of the β 2 Adrenergic Receptor-G_s Protein Complex. *Nature* **2011**, *477*, 549-555.
44. Rasmussen, S. G. F.; Choi, H. J.; Fung, J. J.; Pardon, E.; Casarosa, P.; Chae, P. S.; DeVree, B. T.; Rosenbaum, D. M.; Thian, F. S.; Kobilka, T. S.; Schnapp, A.; Konetzki, I.; Sunahara, R. K.; Gellman, S. H.; Pautsch, A.; Steyaert, J.; Weis, W. I.; Kobilka, B. K., Structure of a Nanobody-Stabilized Active state of the β (2) Adrenoceptor. *Nature* **2011**, *469*, 175-180.
45. Haga, K.; Kruse, A. C.; Asada, H.; Yurugi-Kobayashi, T.; Shiroishi, M.; Zhang, C.; Weis, W. I.; Okada, T.; Kobilka, B. K.; Haga, T.; Kobayashi, T., Structure of the Human M2 Muscarinic Acetylcholine Receptor Bound to an Antagonist. *Nature* **2012**, *482*, 547-551.
46. Manglik, A.; Kruse, A. C.; Kobilka, T. S.; Thian, F. S.; Mathiesen, J. M.; Sunahara, R. K.; Pardo, L.; Weis, W. I.; Kobilka, B. K.; Granier, S., Crystal Structure of the Micro-Opioid Receptor Bound to a Morphinan Antagonist. *Nature* **2012**, *485*, 321-326.
47. Huang, W.; Manglik, A.; Venkatakrisnan, A. J.; Laeremans, T.; Feinberg, E. N.; Sanborn, A. L.; Kato, H. E.; Livingston, K. E.; Thorsen, T. S.; Kling, R. C.; Granier, S.; Gmeiner, P.; Husbands, S. M.; Traynor, J. R.; Weis, W. I.; Steyaert, J.; Dror, R. O.; Kobilka, B. K., Structural Insights into μ -Opioid Receptor Activation. *Nature* **2015**, *524*, 315-321.
48. Tiwary, P.; Parrinello, M., A Time-Independent Free Energy Estimator for Metadynamics. *J. Phys. Chem. B* **2015**, *119*, 736-742.
49. Crombie, A. L.; Antrilli, T. M.; Campbell, B. A.; Crandall, D. L.; Failli, A. A.; He, Y.; Kern, J. C.; Moore, W. J.; Nogle, L. M.; Trybulski, E. J., Synthesis and Evaluation of Azabicyclo[3.2.1]octane Derivatives as Potent Mixed Vasopressin Antagonists. *Bioorg. Med. Chem. Lett.* **2010**, *20*, 3742-3745.
50. Matthews, J. M.; Hoekstra, W. J.; Dyatkin, A. B.; Hecker, L. R.; Hlasta, D. J.; Poulter, B. L.; Andrade-Gordon, P.; de Garavilla, L.; Demarest, K. T.; Ericson, E.; Gunnet, J. W.; Hageman,

W.; Look, R.; Moore, J. B.; Reynolds, C. H.; Maryanoff, B. E., Potent Nonpeptide Vasopressin Receptor Antagonists Based on Oxazino- and Thiazinobenzodiazepine Templates. *Bioorg. Med. Chem. Lett.* **2004**, *14*, 2747-2752.

51. Jean-Alphonse, F.; Perkovska, S.; Frantz, M. C.; Durroux, T.; Mejean, C.; Morin, D.; Loison, S.; Bonnet, D.; Hibert, M.; Mouillac, B.; Mendre, C., Biased Agonist Pharmacochaperones of the AVP V2 Receptor May Treat Congenital Nephrogenic Diabetes Insipidus. *J. Am. Soc. Nephrol.* **2009**, *20*, 2190-2203.

52. Serradeil-Le Gal, C., An Overview of SR121463, a Selective Non-Peptide Vasopressin V(2) Receptor Antagonist. *Cardiovasc. Drug Rev.* **2001**, *19*, 201-214.

53. Rasmussen, S. G.; Choi, H. J.; Fung, J. J.; Pardon, E.; Casarosa, P.; Chae, P. S.; Devree, B. T.; Rosenbaum, D. M.; Thian, F. S.; Kobilka, T. S.; Schnapp, A.; Konetzki, I.; Sunahara, R. K.; Gellman, S. H.; Pautsch, A.; Steyaert, J.; Weis, W. I.; Kobilka, B. K., Structure of a Nanobody-Stabilized Active State of the $\beta(2)$ Adrenoceptor. *Nature* **2011**, *469*, 175-180.

54. Hoffmann, C.; Leitz, M. R.; Oberdorf-Maass, S.; Lohse, M. J.; Klotz, K. N., Comparative Pharmacology of Human β -Adrenergic Receptor Subtypes-Characterization of Stably Transfected Receptors in CHO Cells. *Naunyn-Schmiedeberg's Arch. Pharmacol.* **2004**, *369*, 151-159.

55. Ring, A. M.; Manglik, A.; Kruse, A. C.; Enos, M. D.; Weis, W. I.; Garcia, K. C.; Kobilka, B. K., Adrenaline-Activated Structure of $\beta(2)$ -Adrenoceptor Stabilized by an Engineered Nanobody. *Nature* **2013**, *502*, 575-579.

56. Miao, Y.; Feher, V. A.; McCammon, J. A., Gaussian Accelerated Molecular Dynamics: Unconstrained Enhanced Sampling and Free Energy Calculation. *J. Chem. Theory Comput.* **2015**, *11*, 3584-3595.

57. Lindorff-Larsen, K.; Piana, S.; Palmo, K.; Maragakis, P.; Klepeis, J. L.; Dror, R. O.; Shaw, D. E., Improved Side-Chain Torsion Potentials for the Amber ff99SB Protein Force Field. *Proteins* **2010**, *78*, 1950-1958.

58. Siu, S. W.; Vacha, R.; Jungwirth, P.; Bockmann, R. A., Biomolecular Simulations of Membranes: Physical Properties from Different Force Fields. *J. Chem. Phys.* **2008**, *128*, 125103.

59. Lomize, M. A.; Lomize, A. L.; Pogozheva, I. D.; Mosberg, H. I., OPM: Orientations of Proteins in Membranes Database. *Bioinf.* **2006**, *22*, 623-625.

60. Wolf, M. G.; Hoefling, M.; Aponte-Santamaria, C.; Grubmuller, H.; Groenhof, G., g_membed: Efficient Insertion of a Membrane Protein into an Equilibrated Lipid Bilayer with Minimal Perturbation. *J. Comput. Chem.* **2010**, *31*, 2169-2174.

61. Wang, J.; Wolf, R. M.; Caldwell, J. W.; Kollman, P. A.; Case, D. A., Development and Testing of a General Amber Force Field. *J. Comput. Chem.* **2004**, *25*, 1157-1174.

62. Jakalian, A.; Jack, D. B.; Bayly, C. I., Fast, Efficient Generation of High-Quality Atomic Charges. AM1-BCC Model: II. Parameterization and Validation. *J. Comput. Chem.* **2002**, *23*, 1623-1641.

63. Darden, T.; York, D.; Pedersen, L., Particle Mesh Ewald - an N.Log(N) Method for Ewald Sums in Large Systems. *J. Chem. Phys.* **1993**, *98*, 10089-10092.

64. Berendsen, H. J. C.; Grigera, J. R.; Straatsma, T. P., The Missing Term in Effective Pair Potentials. *J. Phys. Chem.* **1987**, *91*, 6269-6271.
65. Pronk, S.; Pall, S.; Schulz, R.; Larsson, P.; Bjelkmar, P.; Apostolov, R.; Shirts, M. R.; Smith, J. C.; Kasson, P. M.; van der Spoel, D.; Hess, B.; Lindahl, E., GROMACS 4.5: A High-Throughput and Highly Parallel Open Source Molecular Simulation Toolkit. *Bioinf.* **2013**, *29*, 845-854.
66. Tribello, G. A.; Bonomi, M.; Branduardi, D.; Camilloni, C.; Bussi, G., Plumed 2: New Feathers for an Old Bird. *Comput. Phys. Commun.* **2014**, *185*, 604-613.
67. Kling, R. C.; Lanig, H.; Clark, T.; Gmeiner, P., Active-State Models of Ternary GPCR Complexes: Determinants of Selective Receptor-G-Protein Coupling. *PLoS one* **2013**, *8*, e67244.
68. Warne, T.; Moukhametzianov, R.; Baker, J. G.; Nehme, R.; Edwards, P. C.; Leslie, A. G.; Schertler, G. F.; Tate, C. G., The Structural Basis for Agonist and Partial Agonist Action on a $\beta(1)$ -Adrenergic Receptor. *Nature* **2011**, *469*, 241-244.
69. Warne, T.; Edwards, P. C.; Leslie, A. G.; Tate, C. G., Crystal Structures of a Stabilized $\beta 1$ -Adrenoceptor Bound to the Biased agonists Bucindolol and Carvedilol. *Structure* **2012**, *20*, 841-849.
70. Barducci, A.; Bussi, G.; Parrinello, M., Well-Tempered Metadynamics: A Smoothly Converging and Tunable Free-Energy Method. *Phys. Rev. Lett.* **2008**, *100*, 020603.
71. White, J. F.; Noinaj, N.; Shibata, Y.; Love, J.; Kloss, B.; Xu, F.; Gvozdenovic-Jeremic, J.; Shah, P.; Shiloach, J.; Tate, C. G.; Grishammer, R., Structure of the Agonist-Bound Neurotensin Receptor. *Nature* **2012**, *490*, 508-513.
72. Shen, M. Y.; Sali, A., Statistical Potential for Assessment and Prediction of Protein Structures. *Prot. Sci.* **2006**, *15*, 2507-2524.
73. Eswar, N.; Eramian, D.; Webb, B.; Shen, M. Y.; Sali, A., Protein Structure Modeling with MODELLER. *Meth. Mol. Biol.* **2008**, *426*, 145-159.
74. Eisenberg, D.; Luthy, R.; Bowie, J. U., VERIFY3D: Assessment of Protein Models with Three-Dimensional Profiles. *Meth. Enzymol.* **1997**, *277*, 396-404.
75. Gracy, J.; Chiche, L.; Sallantin, J., Improved Alignment of Weakly Homologous Protein Sequences Using Structural Information. *Prot. Eng.* **1993**, *6*, 821-829.
76. Deng, Y.; Roux, B. Calculation of Standard Binding Free Energies: \square Aromatic Molecules in the T4 Lysozyme L99A Mutant. *J. Chem. Theory Comput.*, **2012**, *8*, 1165-1170.
77. Deng, Y.; Roux, B. Computations of Standard Binding Free Energies with Molecular Dynamics Simulations. *J. Phys. Chem. B* **2009**, *113*, 2234-2246.